© 2018. Published by The Company of Biologists Ltd | Development (2018) 145, dev166348. doi:10.1242/dev.166348

RESEARCH ARTICLE

Variant PRC1 competes with retinoic acid-related signals to repress *Meis2* in the mouse distal forelimb bud

Nayuta Yakushiji-Kaminatsui[1,*,‡], Takashi Kondo[1,2,3], Ken-ichi Hironaka[4], Jafar Sharif[1,2], Takaho A. Endo[5], Manabu Nakayama[6], Osamu Masui[1,2], Yoko Koseki[1,2], Kaori Kondo[1,2,3], Osamu Ohara[5,6], Miguel Vidal[7], Yoshihiro Morishita[8] and Haruhiko Koseki[1,2,‡]

ABSTRACT

Suppression of Meis genes in the distal limb bud is required for proximal-distal (PD) specification of the forelimb. Polycomb group (PcG) factors play a role in downregulation of retinoic acid (RA)-related signals in the distal forelimb bud, causing Meis repression. It is, however, not known whether downregulation of RA-related signals and PcG-mediated proximal gene repression are functionally linked. Here, we reveal that PcG factors and RA-related signals antagonize each other to polarize *Meis2* expression along the PD axis in mouse. Supported by mathematical modeling and simulation, we propose that PcG factors are required to adjust the threshold for RA-related signaling to regulate *Meis2* expression. Finally, we show that a variant Polycomb repressive complex 1 (PRC1), incorporating PCGF3 and PCGF5, represses *Meis2* expression in the distal limb bud. Taken together, we reveal a previously unknown link between PcG proteins and downregulation of RA-related signals to mediate the phase transition of *Meis2* transcriptional status during forelimb patterning.

KEY WORDS: *Meis2*, Polycomb, Threshold, Retinoic acid signaling, Forelimb bud, Mouse

INTRODUCTION

Polycomb group (PcG) proteins form two major multimeric protein complexes known as PRC1 and 2 (polycomb repressive complexes 1 and 2) (Simon and Kingston, 2009). Both complexes are evolutionarily conserved from metazoans to mammals, and play synergistic roles to repress developmental genes, such as the Hox cluster. PRC1 mediates histone H2A mono-ubiquitylation at lysine 119 (H2AK119ub1) via E3 ubiquitin ligase activity by RING1A and 1B (RING finger protein 1A and 1B; also known as RING1 and RNF2, respectively), whereas PRC2 mediates histone H3 lysine 27 methylation (H3K27me1/2/3) by the function of EZH1 and 2 (enhancer of zeste homologs 1 and 2). The H3K27me3 marks are further recognized by the PRC1 components CBX2, 4, 6, 7 or 8 (chromobox protein 2, 4, 6, 7 or 8), in turn leading to robust gene repression.

PRC1, furthermore, constitutes six subcomplexes, each incorporating different combinations of PCGF (polycomb group ring finger) proteins (PCGF1 to 6) (Farcas et al., 2012; Gao et al., 2012; He et al., 2013; Wu et al., 2013). The canonical PRC1 (cPRC1) complexes contain PCGF2 (MEL18) or PCGF4 (BMI1) and bind H3K27me3 via the CBX proteins (Aranda et al., 2015; Blackledge et al., 2015; Isono et al., 2013; Kondo et al., 2016). A variant (or non-canonical) PRC1 (vPRC1 or ncPRC1), containing PCGF1, localizes to CpG islands (CGIs) and mediates H2Aub1 (Blackledge et al., 2014). A different vPRC1 complex, containing PCGF3 and 5 (PCGF3/5-PRC1), mediates H2Aub1 and H3K27me3 at the inactive X chromosome (Almeida et al., 2017). Finally, another variant PRC1 complex, containing PCGF6 (PCGF6-PRC1), mediates H2Aub1 and H3K27me3 at meiosis- and/or germ cell-related gene promoters (Endoh et al., 2017).

The role for PcG factors in patterning and cellular differentiation, by repressing developmental genes, is well established. Similarly, it is also well known that morphogenetic signals, such as retinoic acid (RA) or RA-related molecules synthesized by fetal tissues, play a role in the activation of genes during development (Cunningham and Duester, 2015). Based on these arguments, it could be hypothesized that PcG factors and developmental signals oppose each other to regulate gene repression, or activation. During limb development, strong RA-related signals facilitate proximal specification of forelimb bud by activating the Meis (Meis homeobox) genes, such as *Meis2* and *Meis1*, whereas weak RA signals are insufficient to activate Meis, resulting in the progression of distal specification, although this model remains controversial (Cunningham et al., 2013; Mercader et al., 2000; Probst et al., 2011; Rosello-Diez et al., 2014; Yashiro et al., 2004). Our recent study, however, showed that PcG factors repress *Meis2* to mediate distal specification of the forelimb bud where RA-related signals are weak (Yakushiji-Kaminatsui et al., 2016). Therefore, the *Meis2* gene provides an excellent system to probe the competitive relationship between PcG factors and developmental signals.

Here, we examined whether RA-related signals and PcG factors antagonize each other with respect to *Meis2* regulation during proximal-distal (PD) specification of forelimb bud. Indeed, we show that RING1 proteins competitively regulate RA-related signaling to polarize *Meis2* expression along the PD axis. Based on mathematical modeling and simulation, we propose that RING1 adjusts the threshold of RA-related signals for Meis gene regulation. We further sought to

[1]Laboratory for Developmental Genetics, RIKEN Center for Integrative Medical Sciences (RIKEN-IMS), 1-7-22 Suehiro-cho, Tsurumi-ku, Yokohama 230-0045, Japan. [2]JapanCREST, Japan Science and Technology Agency. [3]KAST, Project on Health and Anti-aging, 3-25-13 Tonomachi, Kawasaki-ku, Kawasaki 210-0821, Japan. [4]Department of Biological Sciences, Graduate School of Science, The University of Tokyo, 113-0033, Japan. [5]Laboratory for Integrative Genomics, RIKEN Center for Integrative Medical Sciences (RIKEN-IMS), 1-7-22 Suehirocho, Tsurumi-ku, Yokohama 230-0045, Japan. [6]Department of Technology Development, Kazusa DNA Research Institute, 2-6-7 Kazusa-Kamatari, Kisarazu, Chiba 292-0818, Japan. [7]Centro de Investigaciones Biológicas, Department of Cellular and Molecular Biology, Ramiro de Maeztu 9, Madrid 28040, Spain. [8]Laboratory for Developmental Morphogeometry, RIKEN Center for Biosystems Dynamics Research, 2-2-3 Minatojima-minamimachi, Chuo-ku, Kobe, Hyogo 650-0047, Japan.
*Present address: Division of Immunobiology, Research Institute for Biomedical Sciences, Tokyo University of Science, 2669 Yamazaki, Noda, Chiba 278-0022, Japan.

‡Authors for correspondence (nayuta.yakushiji@rs.tus.ac.jp; haruhiko.koseki@riken.jp)

N.Y.-K., 0000-0001-7324-1161; H.K., 0000-0001-8424-5854

Received 4 April 2018; Accepted 28 August 2018

Development (2018) 145, dev166348. doi:10.1242/dev.166348

clarify the specific PRC1 subtype(s) that are involved in mediation of *Meis2* downregulation in the distal forelimb bud. By performing genetic analyses, we reveal that the variant PCGF3/5-PRC1 complex is required for *Meis2* repression. Taken together, we have discovered a role for PcG factors (i.e. PCGF3/5-PRC1) in repression of *Meis2* expression by creating *de novo* PcG-repressive domain(s) through antagonizing RA-related developmental signals.

RESULTS

RA mediates eviction of PcG factors at the *Meis2* locus in the distal forelimb bud

We investigated whether PcG-mediated repression and RA-related signaling are mutually linked at the *Meis2* locus. Previous reports show that the *Meis2* promoter is bound by retinoic acid receptors (RARs) in F9 embryonal carcinoma cells, inducing transcriptional activation (Chatagnon et al., 2015; Leid et al., 1992; Mangelsdorf and Evans, 1995) (Fig. 1A, tracks 1, 2). Consistent with this notion, we found that RARs bound the *Meis2* promoter region in embryonic day (E) 11.5 embryos in the proximal forelimb bud, but much less so in the distal forelimb bud, reflecting the active status of *Meis2* expression specifically in the proximal forelimb bud (Fig. 1A, tracks 3, 4). We further investigated local enrichment of H3K27 acetylation (H3K27ac), which is known to be mediated by co-activators such as p300 (Ep300) and CBP (CREBBP) that form complexes with RARs in an RA-dependent manner (Tie et al., 2009). Consistent with these findings, a study by McKeown et al. (2017) using human cell lines revealed that local enrichments of H3K27ac and RARs were concurrently induced by an RARα agonist at their common targets, including *MEIS2* and *MEIS1* (McKeown et al., 2017) (Fig. S1A,B). Of note, RAR-mediated signals may mediate local H3K27ac by stimulating co-activators. We did indeed observe considerable enrichment of H3K27ac at the promoter of *Meis2* in the proximal forelimb bud, but depletion of the same mark in the distal forelimb bud (Fig. 1A, tracks 5, 6). These findings suggest that RA-related signals upregulate *Meis2* expression via activation of an RAR/co-activator pathway in the proximal forelimb bud (Bajpe et al., 2013; Chen et al., 2013; Jin et al., 2011).

In contrast, our previous report (Yakushiji-Kaminatsui et al., 2016) showed RING1B binding at the *Meis2* locus, causing transcriptional repression in the distal forelimb bud (Fig. 1A, tracks 7, 8). We therefore investigated whether this inverse correlation between RA-related signals and PcG activity at the *Meis2* locus in developing forelimb bud is functionally interlinked. To this end, we orally administered all-trans RA (ATRA) at a dose of 100 mg/kg to pregnant females at E10.25 (Fig. 1B, left). ATRA administration induced ectopic *Meis2* expression in the distal forelimb buds (Fig. 1B, right), in combination with decreases in both RING1B (PRC1 component) binding and H3K27me3 (indicator of PRC2 activity) deposition at the *Meis2* promoter in the distal forelimb bud (Fig. 1C, top). Similarly, RING1B binding and H3K27me3 levels were also downregulated in the RING1B binding site at the 3′ region of the *Meis2* (RBS). The RBS associates with the repressed promoter and facilitates RING1B binding (Fig. 1C, top) (T.K., Y.K. and H.K., unpublished observations). We further confirmed whether ATRA treatment activates the RAR/co-activator pathway at *Meis2*. We investigated local H3K27ac levels, which correlate with RA signal intensity (Fig. S1A,B), and found a considerable increase in H3K27ac in the distal forelimb bud (Fig. 1C, bottom). We also found an increase in another activating mark, H3K4 trimethylation (H3K4me3) (Fig. 1C, bottom). Collectively, these data indicate that activation of the RAR/co-activator pathway contributes to the eviction of PcG factors from the *Meis2* locus.

We went on to investigate whether ATRA-mediated PcG eviction affects the contact between promoter and RBS in the *Meis2* locus, which is mediated by RING1 proteins (Kondo et al., 2014; Yakushiji-Kaminatsui et al., 2016) (Fig. 1D). We used the DNA-FISH technique to measure the distance between promoter and RBS and found that the promoter-RBS contact was dissolved in the distal forelimb bud by ATRA treatment (Fig. 1D). These findings support the model that *Meis2* activation in the distal forelimb bud by strong RA signals involves eviction of PcG factors.

To validate the role of endogenous RA-related signals in eviction of PcG factors, we took advantage of a loss of function of CYP26B1 mutant (*Cyp26b1* KO), which shows sustained RA signaling throughout the limb bud due to a block in degradation of endogenous RA or its related molecules (Yashiro et al., 2004). Consistent with our hypothesis that ATRA mediates eviction of PcG, we observed depletion of RING1B binding and H3K27me3 at both promoter and RBS regions in distal forelimb buds in the *Cyp26b1* KO (Fig. 1E), which was reminiscent of the alterations in PcG enrichment seen in the ATRA-treated distal forelimb buds (Fig. 1C, top). Taken together, these data further support the notion that endogenous RA-related signals mediate polarization of *Meis2* expression (i.e. create *Meis2*-positive or -negative domains) in forelimb bud by inhibiting PcG activity.

ATRA-mediated PcG eviction occurs at *Meis* but not *Pitx2* or *Hoxa11/13* gene loci in the forelimb bud

We investigated whether ATRA-mediated signals are linked with PcG activity in general or in a locus-specific manner at PcG target genes during PD specification. We selected *Meis1*, *Pitx2*, *Hoxa11* and *Hoxa13* genes, which exhibit proximally or distally skewed expression, and are targeted by both PcG factors and RARs in the forelimb bud at E11.5 (Fig. S1C). *Meis1* is structurally related to *Meis2* and shows strong RAR binding and H3K27ac enrichment at the proximal forelimb bud. In contrast, RING1B is enriched at the distal forelimb bud, similar to *Meis2* (Fig. S1C, left). Furthermore, we have previously shown that *Meis1* is repressed in the distal forelimb bud in a PcG-dependent manner, but is activated by ATRA administration (GSM1716758, published microarray data; Yakushiji-Kaminatsui et al., 2016). The *Pitx2* gene is also bound by RARs and H3K27ac in the proximal forelimb bud, but repressed by RING1 in the distal forelimb bud (Fig. S1C, middle). Unlike *Meis2*, however, *Pitx2* is not activated by ATRA (GSM1716758, published microarray data; Yakushiji-Kaminatsui et al., 2016). The *Hoxa11/13* genes, located at the 3′ region of the *HoxA* gene cluster, are bound by H3K27ac in the distal forelimb bud and by RING1B in the proximal forelimb bud, but do not show enrichment of RARs (Fig. 1C, right). In addition, *Hoxa11/13* genes are expressed in the distal forelimb bud, and are downregulated by ATRA, likely via RAR binding to the 5′ region of *HoxA* cluster (GSM1716758, published microarray data; Yakushiji-Kaminatsui et al., 2016).

We compared RING1B, H3K27me3, H3K4me3 and H3K27ac levels at the above genes, and observed reduction of RING1B and H3K27me3 at both promoter and RBS regions of *Meis1*, similar to observations with respect to *Meis2* (Fig. S1D). However, binding of RING1B or H3K27me3 did not change at *Pitx2*, *Hoxa11* and *Hoxa13* promoters upon ATRA treatment, in either proximal or distal forelimb bud (Fig. S1E). Intriguingly, H3K4me3 and H3K27ac levels were differentially regulated at these genes, indicating that the effect of ATRA on these genes is not necessarily the same (Fig. S1C,D). Taken together, our data show that target binding of PcG factors is sensitive to RA-related signals at specific gene loci, such as *Meis2* and *Meis1*, in the forelimb bud.

Development (2018) 145, dev166348. doi:10.1242/dev.166348

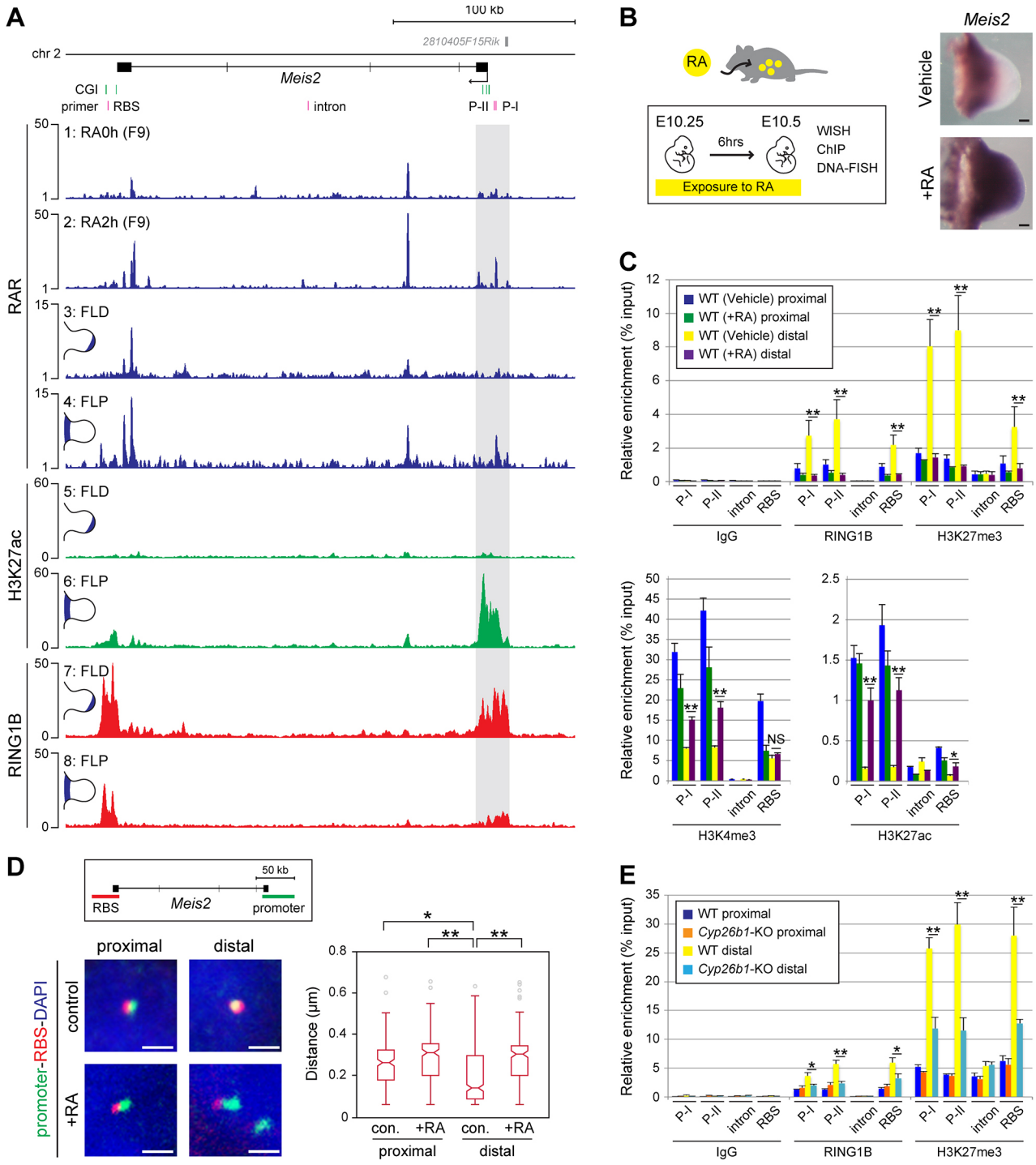

Fig. 1. See next page for legend.

PcG factors regulate ATRA sensitivity of *Meis2* in the forelimb bud

The above evidence clearly indicates that RA-related signals negatively regulate PcG function at Meis genes. Reciprocally, PcG factors regulate RA sensitivity of Hox genes and *Stra8* (Bel-Vialar et al., 2000; Yokobayashi et al., 2013). Our previous report, showing RING1-dependent modulation of RA sensitivity during PD specification of forelimb bud (Yakushiji-Kaminatsui et al., 2016), is consistent with these notions.

By using the *Meis2* gene as a model, we sought to clarify whether RA sensitivity in forelimb bud could be inversely regulated by PcG factors. We challenged *Ring1B* conditional knockout mutants (*Prx1-Cre;Ring1B*$^{fl/+}$ or *Prx1-Cre;Ring1B*$^{fl/fl}$) or control (*Ring1B*$^{fl/+}$ or *Ring1B*$^{fl/fl}$) embryos (E10.5) with ATRA by maternal oral gavage (5 mg/kg). At this dose, we observed, by *in situ* hybridization, ectopic activation of the *Meis2* gene in a part of the control forelimb bud (Fig. 2A). We obtained control and mutant embryos by crossing *Ring1B*$^{fl/fl}$ females with *Prx1-Cre;Ring1B*$^{fl/+}$ males. Six hours after ATRA administration, four out of 11 control embryos exhibited subtle upregulation of *Meis2* in the distal limb bud (Fig. 2A, bottom left). *Prx1-Cre;Ring1B*$^{fl/+}$ embryos showed more pronounced expansion of the *Meis2* expression domain (n=9/14) (Fig. 2A,

Development (2018) 145, dev166348. doi:10.1242/dev.166348

Fig. 1. RING1 activity at the *Meis2* gene is disturbed by excess RA-related signals. (A) Distribution of RAR, H3K27ac and RING1B at the *Meis2* locus in F9 cells (RA0h, vehicle only) and 2 h after RA stimulation (RA2h), and in E11.5 proximal (FLP) and distal (FLD) forelimb buds revealed by ChIP-seq analysis. The genomic region bound by RING1B, including CpG island and the promoter, is shaded. More intense enrichment of RAR and H3K27ac was detected in the proximal region (FLP) whereas RING1B was enriched in the distal region (FLD). CpG islands (CGI) and the position of ChIP primers are shown by green and red vertical lines, respectively. Schematics in track 3-8 represent the portion of forelimb buds (shown in blue) that were used for the ChIP experiment. Enrichment of ChIP-seq (*y*-axis) is shown as the normalized depth of coverage. (B) All-trans RA-dependent activation of *Meis2* in the distal forelimb bud. Experimental schemes for ATRA treatment (left) and *Meis2* expression in the vehicle- and ATRA-treated (+RA) forelimb buds at E10.5 (right) are shown. Forelimb buds are oriented with proximal to the left and distal to the right. Scale bars: 100 µm. (C) ATRA-dependent reduction in accumulation of RING1B and H3K27me3 around the promoters and RBS of the *Meis2* locus in the distal forelimb buds. Positions of genomic regions tested for respective binding are shown in A. Presence of RING1B, H3K27me3, H3K4me3 and H3K27ac at P-I and P-II, which are located around the TSS, the intronic region and RBS were compared between the wild type (vehicle) and ATRA-treated wild type (+RA) in proximal and distal regions of E10.5 forelimb buds (bottom). Error bars indicate s.e.m. of two or three biological replicates. $^{**}P<0.01$, $^{*}P<0.05$, NS>0.05, Student's *t*-test. (D) Dissolution of promoter/RBS association in the distal forelimb buds by ATRA treatment. Genomic regions used as FISH probes are schematically illustrated (left top). The subnuclear localization of promoter (green) and RBS (red) regions was examined in the proximal and distal regions of control (*Ring1A*-KO) and ATRA-treated wild-type (+RA) forelimb bud at E10.5 (left bottom). The box plots represent the interprobe distances in each forelimb bud region. Median values (middle bars) and first to third interquartile ranges (boxes); whiskers indicate 1.5× the interquartile ranges; dots indicate outliers. Over 200 loci were observed in respective experiments. $^{**}P<10^{-300}$, $^{*}P=2.1\times10^{-15}$, Student's *t*-test. Scale bars: 1 µm. (E) Reduction of RING1B and H3K27me3 enrichment in the distal region of *Cyp26b1*-KO forelimb buds at E10.5. Error bars indicate s.e.m. of three biological replicates. $^{**}P<0.01$, $^{*}P<0.05$, Student's *t*-test.

bottom middle). In contrast, *Prx1-Cre;Ring1B*$^{fl/fl}$ (*Ring1B*-KO) embryos showed robust expansion of the *Meis2* expression domain reaching as far as the distal tip of forelimb buds (n=10/11) (Fig. 2A, bottom right). Therefore, sensitivity of *Meis2* expression to RA signals is enhanced in the *Ring1B* mutants, indicating a reciprocal role for PcG factors in regulation of RA function (Fig. 2A).

To rule out the possibility that the phenotype described above arises from alteration of RA-related signals along the PD axis, we took advantage of a *RARE-lacZ* reporter allele (Rossant et al., 1991), which is a standard indicator for RA-related signals. Indeed, we found no obvious changes in the *lacZ* expression pattern in the *Ring1A/B*-dKO forelimb bud (Fig. 2B). Based on these results, we concluded that PcG factors limit RA-related signal transduction at *Meis2*. Taken together, the above observations indicate that RA-related signals and PcG activity compete with each other to regulate *Meis2* expression in the forelimb bud and polarize the transcription of *Meis2* along the PD axis.

PcG factors adjust the threshold of RA-related signals at *Meis2*

To further explore the potential role of PcG factors in competitive regulation of RA-related signals at *Meis2*, we performed mathematical modeling. To this end, we defined the reciprocal properties between RA-related signals and RING1 as components of a classical chemical reaction, delineated by the formula shown below (Fig. 2C):

$$[\mathrm{Meis}] \propto \frac{[\mathrm{RA}]^h}{[RA]^h + [PcG]^h + K^h}.$$

Here, [X] indicates the concentration of chemical X, and K and h are reaction constants (Lehninger, 1970). The expression level of *Meis2* in each cell is defined by an input [RA], and a threshold $(K')^h$. The input [RA] depends on the position of the cell along the PD axis. $(K')^h$ represents the sum of $[\mathrm{PcG}]^h$ and K^h, and acts as a threshold for regulation of *Meis2* expression (Fig. 2C). RING1B is uniformly expressed along the PD axis (Yakushiji-Kaminatsui et al., 2016), indicating that the threshold $(K')^h$ is constant, independent of the position of cells within the forelimb bud. Thus, for a given RA gradient, the expression level of RING1 should adjust the threshold of RA-related signaling and determine the *Meis2* expression region along the PD axis. Conversely, in the *Ring1* mutant, the affinity of RA-related signals for the regulatory regions of *Meis2* will increase in each cell throughout the limb bud (shown by a green arrow in Fig. 2C). This model is also consistent with our experimental observations (Fig. 2A).

We asked whether this model could explain the respective gene expression patterns in wild-type or control (*Ring1A*-KO), ATRA-treated wild-type, *Ring1A/B*-dKO and *Prx1-Cre;Ring1A*$^{-/-}$*;Ring1B*$^{fl/fl}$*;Meis2*$^{fl/fl}$ (*Ring1A/B;Meis2*-tKO) forelimb buds. To this end, we took advantage of a previously proposed network involving RA-related signals, CYP26B1 and FGF activities during early PD specification (Probst et al., 2011). In this network, we included the RING1 proteins as threshold adjusters for *Meis1/2* expression. We considered both *Meis2* and *Meis1* genes, because both are regulated by RA-related signals and inhibit distal specification (Capdevila et al., 1999; Mercader et al., 2009). We further developed our model by combining the following interactions (i-vii, shown by solid arrows in Fig. 2D) (also see Materials and Methods): *Meis2* is activated by RA-related signals (Mercader et al., 2000) (i); FGFs released from apical ectodermal ridge (AER) activate CYP26B1 expression (ii); the activated CYP26B1 degrades RA (Probst et al., 2011; Yashiro et al., 2004) (iii); Meis2 suppresses the expression of *Cyp26b1* (Rosello-Diez et al., 2014) (iv) and *Fgf8* at AER (figure 4B in Yakushiji-Kaminatsui et al., 2016) (v); Meis2 also suppresses *Hoxa13* (Rosello-Diez et al., 2014; figure 4B in Yakushiji-Kaminatsui et al., 2016) (vi); and PcG factors inhibit Meis1/2 (figure 1E in Yakushiji-Kaminatsui et al., 2016) (vii). Two more potential interactions (indicated by dashed arrows in Fig. 2D), induction of *Hoxa13* by AER-derived FGFs (Vargesson et al., 2001) (viii) and binding of PcG factors to the *Hoxa13* promoter in the proximal forelimb bud (ix), may exist (Fig. S1E). However, we did not include these interactions (viii and ix) in the mathematical modeling because *Hoxa13* induction by AER (viii) was reported to be mediated by RA/Meis axis (Rosello-Diez et al., 2014) and PcG binding to the *Hoxa13* promoter (ix) was permissive to repression mediation in our previous study (Yakushiji-Kaminatsui et al., 2016).

We examined whether our model could recapitulate the expression patterns of *Fgf8*, *Meis1/2* and *Hoxa13* in ATRA-treated wild type, *Ring1A/B*-dKO or *Ring1A/B;Meis2*-tKO mutant forelimb buds (Fig. 2E, also see Table 1). Indeed, computer simulations revealed that ATRA treatment upregulated *Meis1/2* expression in the distal forelimb bud and inhibited distal forelimb-specific genes such as *Fgf8* and *Hoxa13* (Fig. 2E). In the *Ring1A/B*-dKO, lowering the threshold for RA-related signals upregulated *Meis1/2* expression, and downregulated *Fgf8* and *Hoxa13* in the distal forelimb bud (Fig. 2E). Furthermore, in the *Ring1A/B;Meis2*-tKO forelimb bud, *Meis2* depletion, despite sustained expression of *Meis1*, partially restored *Fgf8* and *Hoxa13* levels (Fig. 2E). Collectively, these results support a role of RING1 as a threshold adjuster for RA-related signals to regulate *Meis2* expression in forelimb bud.

Development (2018) 145, dev166348. doi:10.1242/dev.166348

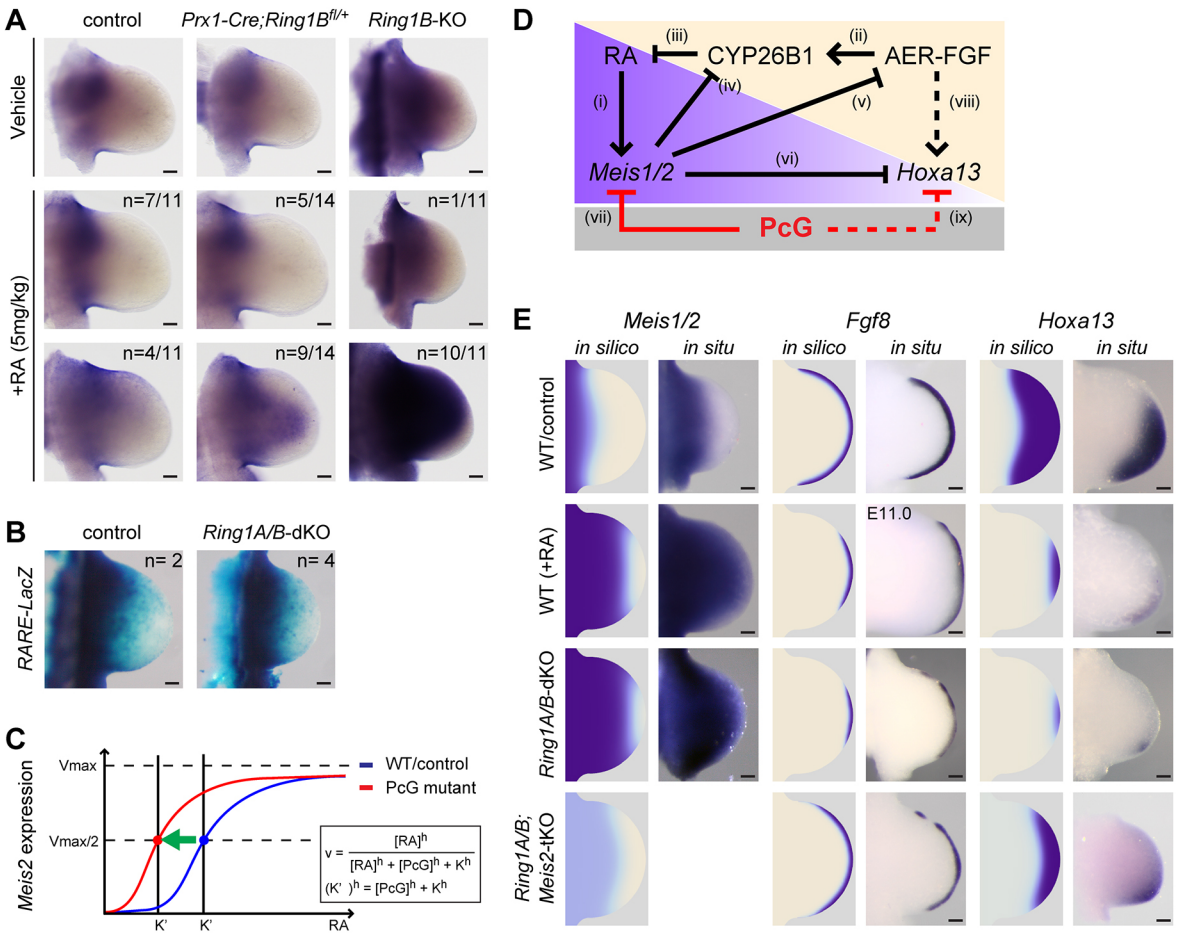

Fig. 2. RING1 activity works as a threshold adjuster for RA signal. (A) *Meis2* expression in the forelimb bud of control (*Ring1B*$^{fl/fl}$ or *Ring1B*$^{fl/+}$), *Prx1-Cre;Ring1B*$^{fl/+}$ and *Ring1B*-KO with either vehicle or ATRA treatment (+RA). Representative *Meis2* expression patterns for each genotype are shown. Forelimb buds are oriented with proximal to the left and distal to the right. Frequency of ATRA-treated specimens exhibiting respective representative *Meis2* expression patterns among each genotype is indicated in each panel. (B) The expression of *RARE-lacZ* transgene in the control (*Ring1A*-KO) and *Ring1A*/*B*-dKO forelimb buds at E10.5. (C) Graphic representation of the deduced relationship between *Meis2* expression and doses of RA-related signals from analyses shown in Figs 1 and 2. The value of *K*′ is thought to depend on the amount of PcG factors. Note the expected shift of the threshold for doses of RA-related signals towards a lower range upon PcG deficiency in comparison with the wild type (represented by a green arrow). *y*-axis represents the reaction rate for *Meis2* activation. (D) A minimal gene regulatory network model for early PD specification including activity of PcG proteins. See the main text for explanations of each pathway. Simulations were performed using only the pathways i-vii represented as solid lines. (E) Expression patterns of *Meis1*/*2*, *Fgf8* and *Hoxa13* obtained from numerical simulations of the gene regulatory network model shown in D (‘*in silico*’) and *in situ* hybridization for wild-type or control (*Ring1A*-KO), ATRA-treated wild-type (+RA), *Ring1A*/*B*-dKO and *Ring1A*/*B;Meis2*-tKO forelimb buds at E10.5 or E11 (*Fgf8* in ATRA-treated forelimb bud). The panels showing *in situ* expression patterns of *Meis2*, *Fgf8* and *Hoxa13* in *Ring1A*/*B*-dKO and *Hoxa13* in *Ring1A*/*B;Meis2*-tKO are taken from our previous study (Yakushiji-Kaminatsui et al., 2016). Scale bars: 100 µm in A,B,E.

PCGF3/5-PRC1 repress *Meis2* in the distal forelimb bud

Having shown that PcG factors play a role in modulation of the threshold of RA-related signaling at *Meis2*, we sought to clarify the specific PRC1 subcomplex(es) that play a role in downregulation of *Meis2* expression. Because different PCGF (1 to 6) proteins give rise to different PRC1 subcomplexes, we surveyed forelimb phenotypes in embryos with each of the six Pcgf genes (*Pcgf1-6*) individually knocked out. Our previous reports indicated that PCGF2, PCGF4 and PCGF6 are dispensable for skeletal patterning of the forelimb, along the PD axis (Akasaka et al., 2001; Endoh et al., 2017; Isono et al., 2005). Therefore, in the present study we explored the role of PCGF1, PCGF3 and PCGF5 in either *Meis2* expression or skeletal patterning of the forelimb by using respective mutant alleles (Fig. S2A,B,D). Deletion of *Pcgf1* at E8.5 did not alter *Meis2* expression in the forelimb buds at E10.5 (Fig. S2A; T.K. and H.K., unpublished observations). Deletion of *Pcgf3* caused perinatal lethality and skeletal defects, in both zeugopod and scapula, similar to the *Ring1B*-KO, and posterior homeotic transformations of the axis (Fig. 3A, Fig. S2B,C). Finally, the *Pcgf5* mutant embryos developed normally to adulthood and showed normal skeletal patterns (Fig. S2D,E; Y.K. and H.K., unpublished observations). Thus, our results reveal that the PCGF3-PRC1 complex mediates PD specification in the forelimb bud.

As PCGF3 and PCGF5 participate in similar protein complexes and possess redundant functions (Almeida et al., 2017; Gao et al., 2012), we deleted both *Pcgf3* and *Pcgf5* to investigate the role of PCGF3/5-PRC1. We first examined *Pcgf3*/*5*-dKO embryos, in which both genes are constitutively depleted, and found them to be embryonic lethal around E9.5 and to exhibit general growth defects at E7.5 (Almeida et al., 2017). We further observed similar phenotypes in *ERT2Cre;Pcgf3*$^{fl/fl}$*;Pcgf5*$^{fl/fl}$ embryos treated with 4-hydroxytamoxifen at the pre-implantation stage (Fig. 3B). We thus used *ERT2Cre;Pcgf3*$^{fl/fl}$*;Pcgf5*$^{fl/fl}$ embryos treated with tamoxifen at E8.5 (*Pcgf3*/*5*-dKO) to examine the roles of *Pcgf3* and

Development (2018) 145, dev166348. doi:10.1242/dev.166348

Table 1. Parameter values used for computer simulations

		WT	dKO	tKO	RA+
RA diffusion	D_R	2.5			
RA decay (basal)	γ_R	0.01			
RA decay (Cyp26b1-dependent)	γ_{RC}	0.1			
RA source level	R_0	1.0			8.0
FGF8 diffusion	D_F	1.0			
FGF8 decay	γ_R	0.025			
FGF8-Meis1/2 dissociation constant	K_{FM}	0.6			
Cyp26b1 max production	α_C/γ_C	1.0			
Cyp26b1-FGF8 dissociation constant	K_{CF}	0.1			
Cyp26b1-Meis1/2 dissociation constant	K_{CM}	0.6			
Meis1/2 maximum production	α_M/γ_M	1.0		0.5	
Meis1/2-PcG dissociation constant	$K_{MR}(P)$	0.25	0.025	0.025	
Hoxa13 maximum production	α_H/γ_H	1.0			
Hoxa13-Meis1/2 dissociation constant	K_{HM}	0.2			
Hill coefficient	h	2.0			

Pcgf5 in the developing forelimb bud and observed considerable expansion of the *Meis2* expression domain in the distal forelimb bud at E10.5 (Fig. 3C). We further noted depletion of H3K27me3 deposition at the *Meis2* promoter in the *Pcgf3/5*-dKO (Fig. 3D). We checked the level of contact between the promoter and RBS at *Meis2*, and found that the promoter and RBS were dissociated in the distal forelimb bud (Fig. 3E). Therefore, the forelimb bud phenotype observed in the *Pcgf3/5*-dKO resembles that of the *Ring1A/B*-dKO. Taken together, PCGF3/5-PRC1 mediates *Meis2* downregulation in distal forelimb bud by inducing a PcG-repressive domain at the *Meis2* locus.

DISCUSSION

We designed the present study to elucidate the interactions between PRC1 and RA-related signals for polarizing *Meis2* gene repression along the PD axis of the forelimb bud, by combining genetic studies on various PRC1 mutants and mathematical modeling. We did indeed find a novel role for the variant PCGF3/5-PRC1 in repression of *Meis2* expression in the distal forelimb bud, likely by adjusting the threshold for RA-related signals (Fig. 3F).

We therefore propose that PCGF3/5-PRC1 possesses two distinct functions: initiation of PcG-mediated silencing of *Meis2*, and sensing of RA-related signals. The first function of PCGF3/5-PRC1 is consistent with our previous observation that showed a role for PCGF3/5-PRC1 in X chromosome inactivation, via recruitment of the PRC2 complex (Almeida et al., 2017; Pintacuda et al., 2017). PCGF3/5-PRC1-mediated *Meis2* repression similarly involves PRC2 recruitment, likely via RING1-dependent H2A mono-ubiquitylation (Blackledge et al., 2014). Another mechanism by which PRC1 could adjust the threshold for RA-related signals was revealed by treating *Ring1B* mutants with ATRA, as well as by a mathematical model in which the threshold-adjuster function is integrated into gene regulatory networks for PD patterning. We find that the computer simulations recapitulate the expression patterns of *Meis1/2*, *Fgf8* and *Hoxa13* at E10.5 under various experimental conditions, and thus support our genetic model. As already mentioned, our model does not consider the degree of tissue outgrowth of the forelimb bud, as the time scale of these biochemical reactions induced by developmental signals (see Fig. 2C) should be much faster than tissue growth. Previous studies, however, indicate that tissue outgrowth and epigenetic changes at target genes could be contributing factors for differentiation of the distal forelimb bud into prospective zeugopod and autopod regions (Rosello-Diez et al., 2014; Uzkudun et al., 2015). Of note, *Meis1/2* genes are stably repressed in the distal forelimb bud (Mercader et al., 2000, 2009). Thus, our study indicates that PcG factors play two distinct roles in the control forelimb specification. First, at the E10.5 forelimb region, PcG factors regulate *Meis1/2* expression as a threshold adjuster of RA-related signals. Second, in the later stages of limb development (post E10.5), PcG factors mediate robust gene repression to lock-down tissue specification stably. Full elucidation of the roles of PcG factors will therefore extend our understanding of PD specification of the forelimb bud.

It is noteworthy that the molecular mechanisms by which PCGF3/5-PRC1 and RA-related signals are linked are not fully understood yet. Our study reveals that ATRA-mediated inhibition of PcG binding at *Meis2* accompanies accumulation of H3K27ac, which is mediated by p300 and CBP co-activators (Jin et al., 2011; Tie et al., 2009) (Fig. 1 and Fig. 3G, left). It is known that RARs interact with both co-activators or co-repressors, in an RA-dependent manner, to facilitate active or repressive chromatin domains, respectively (Chen et al., 1997; Nagy et al., 1997). We thus speculate that in the absence of RA-related signals, or when such signals are less abundant, co-repressors mediate the interactions between PcG factors and RARs. Indeed, co-repressors such as CTBP and histone deacetylases can associate with both RAR complexes and PcG factors, in the absence of exogenous RA (Sánchez et al., 2007; Sewalt et al., 1999; van der Vlag and Otte, 1999). We therefore hypothesize that PCGF3/5-PRC1 cooperates with RARs to form complexes with co-repressors, in the absence of abundant RA-related signals (Fig. 3G, right). Intriguingly, it has been reported that PCGF3/5-PRC1 could also be functionally linked with p300 to mediate gene activation (Zhao et al., 2017). Selective interactions between PCGF3/5-PRC1 and either co-activators or co-repressors that depend on the amount of RA may contribute to polarization of *Meis2* expression in the forelimb bud (Fig. 3G). PCGF3/5-PRC1 may partly mediate the RA-dependent competition between co-activators and co-repressors to adjust the threshold for RA-related signals.

Previous studies have revealed functional interactions between PcG factors and not only RA-related signals but also developmental signal pathways such as Hedgehog, WNT and TGFβ (Boukarabila et al., 2009; Gaarenstroom and Hill, 2014; Marino, 2005). Importantly, these pathways also associate with co-activators in a ligand-dependent manner (Akimaru et al., 1997; Itoh et al., 2000; Roose et al., 1998). Molecular mechanisms that potentially link PcG factors and RARs, in a ligand-dependent manner, to downregulate *Meis2* expression could also be employed in other morphogenetic signal pathways to alter target gene expression during development. Our study, by showing a link between PCGF3/5-PRC1 and developmental regulation of the *Meis2* gene, will therefore contribute to a better understanding of the regulatory mechanisms for developmental signal-dependent recruitment of PcG factors at target genes. Intriguingly, we also show that activities of PcG factors were not affected by excess RA signals at *Pitx2*, *Hoxa11* or *Hoxa13* promotors, suggesting another aspect of PcG activity in protecting CGI promoters from unnecessary developmental signals.

MATERIALS AND METHODS

Animals

All animal experiments were carried out according to the in-house guidelines for the care and use of laboratory animals of the RIKEN, Yokohama Institute, Japan. *Cyp26b1*$^{+/-}$, *RARE-hsplacZ*, *Prx1-Cre; Ring1B*$^{fl/fl}$, *Prx1-Cre;Ring1A*$^{-/-}$*;Ring1B*$^{fl/fl}$ and *Prx1-Cre;Ring1A*$^{-/-}$*;*

Development (2018) 145, dev166348. doi:10.1242/dev.166348

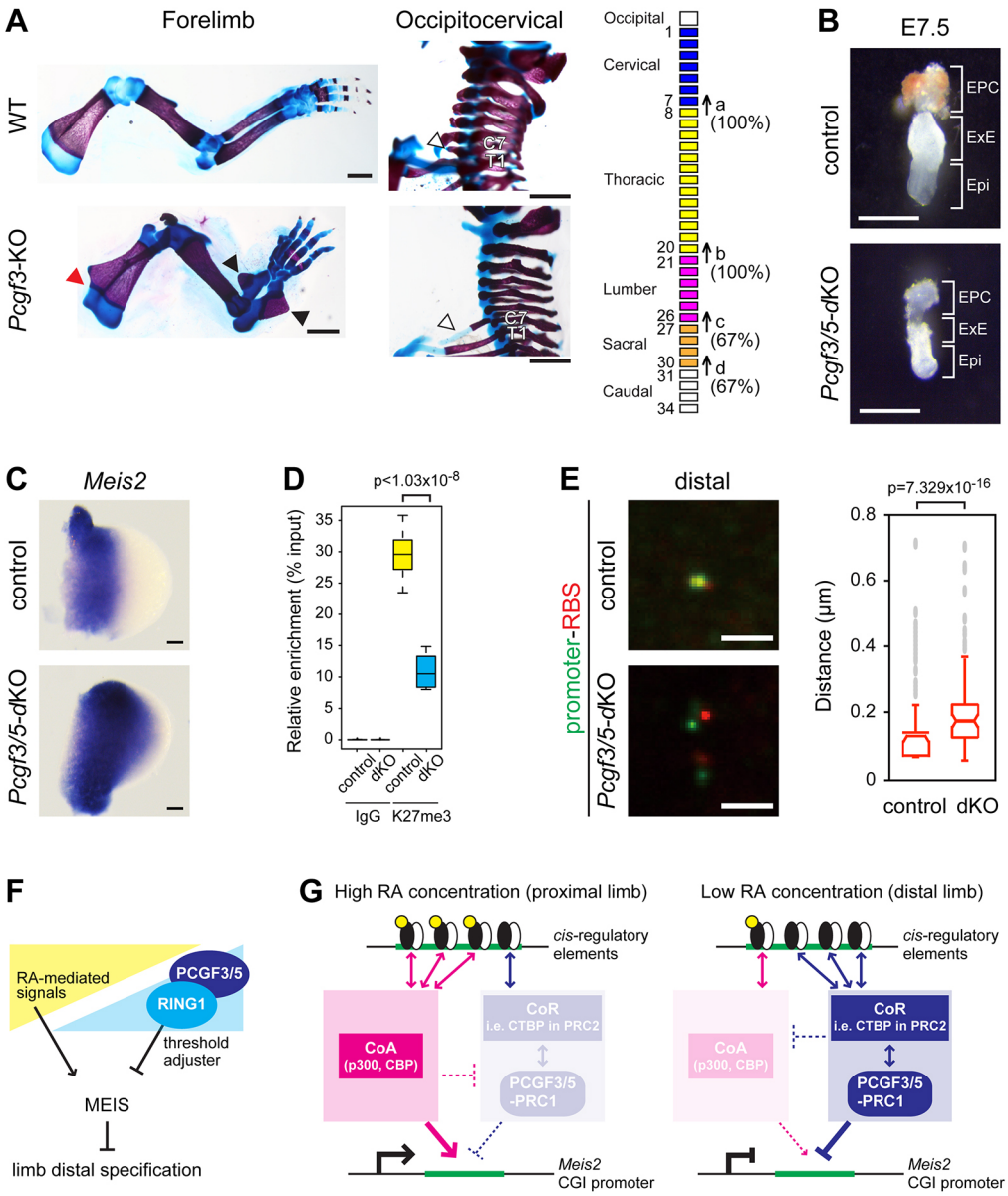

Fig. 3. *Pcgf3/5* deficiency phenocopies mis-regulation of the *Meis2* gene in the forelimb bud. (A) Left-hand panels show the forelimb skeletal pattern of wild type and *Pcgf3*-KO at postnatal day (P) 0. Deformity of scapula (red arrowhead) and shortening of zeugopod (black arrowheads) were observed in *Pcgf3*-KO newborn mice. Middle panels show the axial skeletal changes observed in *Pcgf3*-KO. Lateral views of cervical and upper thoracic regions in wild-type and *Pcgf3*-KO newborn mice (P0) are shown. Note association of rib-like processes with C7 (indicated by white arrowhead) in *Pcgf3*-KO. Schematic shows the posterior transformations in the vertebral column of *Pcgf3*-KO (n=6): (a) C7→T1, appearance of cervical ribs on C7; (b) T13→L1, loss of the thirteenth rib from the 20th vertebra; (c) L6→S1, formation of the sacroiliac joint in the 26th vertebra; (d) S4→Ca1, appearance of the first caudal vertebra in the 30th vertebra. Scale bars: 1 mm. (B) Developmental defects in *ERT2Cre;Pcgf3$^{fl/fl}$;Pcgf5$^{fl/fl}$* (*Pcgf3/5*-dKO) at E7.5. EPC, ectoplacental corn; ExE, extra-embryonic ectoderm; Epi, epiblast. Scale bars: 0.5 mm. (C) Requirement of PCGF3/5 for *Meis2* repression in the distal region of forelimb bud. Forelimb buds are oriented with proximal to the left and distal to the right. Scale bars: 100 µm. (D) Considerable reduction of H3K27me3 enrichment at the TSS of *Meis2* gene in the distal forelimb bud of *Pcgf3/5*-dKO. H3K27me3 levels at P-I, located at the TSS of *Meis2* gene, was compared between control (*Pcgf3$^{fl/fl}$;Pcgf5$^{fl/fl}$*) and *Pcgf3/5*-dKO in distal regions of E10.5 forelimb buds. The box plots show a relative enrichment of percentage input obtained from six biological replicates. P=1.03×10^{-8}, Student's t-test. (E) Dissolution of promoter/RBS interaction in the distal forelimb bud of *Pcgf3/5*-dKO. The subnuclear localization of promoter (green) and RBS (red) regions was examined in the distal forelimb buds of control (*Pcgf3$^{fl/fl}$;Pcgf5$^{fl/fl}$*) and *Pcgf3/5*-dKO at E10.5 (left). The box plots show the interprobe distances in each distal forelimb bud tissue (right). Median values (middle bars) and first to third interquartile ranges (boxes); whiskers indicate 1.5× the interquartile ranges; dots indicate outliers. Over 250 loci were observed in this experiment. P=7.329×10^{-16}, Student's t-test. Scale bar: 1 µm. (F) Schematic of the role of variant PRC1 complexes including RING1 and PCGF3/5 in *Meis2* repression during distal development of forelimb buds likely through adjusting the threshold of RA-related signals. (G) The model for the thresholding adjuster function of variant PCR1 from presented data and previous findings. See Discussion for a description of the model presented. Retinoic acid is depicted as yellow circles and RAR/RXR heterodimer is shown as black and white ovals.

Ring1B$^{fl/fl}$;Meis2$^{fl/fl}$ mouse lines were described previously (Rossant et al., 1991; Yashiro et al., 2004; Yakushiji-Kaminatsui et al., 2016). Generation of *Pcgf3$^{fl/fl}$* and *Pcgf5$^{fl/fl}$* mice is described in Fig. S2B,D. *Pcgf3*-KO mice were obtained by crossing *Pcgf3$^{+/-}$* mice. *Pcgf3/5* double mutant embryos were obtained by mating male *ERT2Cre;Pcgf3$^{fl/fl}$;Pcgf5$^{fl/fl}$* and female *Pcgf3$^{fl/fl}$;Pcgf5$^{fl/fl}$* mice and subsequent intraperitoneal tamoxifen injection. Generation and analysis of *Pcgf1$^{fl/fl}$* mice will be described elsewhere. To induce deletion of *Pcgf1*, *Pcgf3* and/or *Pcgf5*, we injected 0.1 ml of

Development (2018) 145, dev166348. doi:10.1242/dev.166348

15 mg/ml tamoxifen (Sigma-Aldrich) into the peritoneal cavity at E8.5 and sampled embryos at E10.5. *Pcgf3/5* double mutant embryos shown in Fig. 3B were obtained by the following procedure: embryos were generated by *in vitro* fertilization and cultured until the blastocyst stage. To induce deletion of *Pcgf3/5*, embryos at the morula stage were further cultured in KSOM medium with 4-hydroxytamoxifen (7.7 µM, Sigma-Aldrich) for 24 h, followed by transplantation to the foster mothers (E2.5) and sampling at E7.5. Primers used for genotyping of respective alleles are listed in Table S1.

Skeletal preparation, whole-mount *in situ* hybridization and X-gal staining

Skeletons of fetal and newborn mice were stained with Alizarin Red and Alcian Blue as described previously (Parr and McMahon, 1995). Whole-mount *in situ* hybridization was performed according to the methods described by Wilkinson and Nieto (1993). Whole-mount detection of β-galactosidase activity by X-gal staining was carried out as described previously (Loughna and Henderson, 2007).

Retinoic acid treatment and sampling

Retinoic acid (RA) treatment was performed as previously described (Yashiro et al., 2004). Wild-type embryos (BDF2) that were transplanted into ICR female recipients received all-trans RA (ATRA) (Sigma-Aldrich) at a dose of 100 mg/kg body weight in sesame oil (Sigma-Aldrich) at E10.25 by maternal oral administration and were sampled 6 h (E10.5) or 18 h (E11.0) after ATRA treatment. Embryos obtained by crossing *Ring1B*$^{fl/fl}$ females with *Prx1-Cre;Ring1B*$^{fl/+}$ males received ATRA at a dose of 5 mg/kg body weight at around E10.25 and were sampled 6 h (around E10.5) after oral administration. Experimental control pregnant females were administered sesame oil (vehicle) only. These embryos were subjected to *in situ* hybridization, DNA-FISH and ChIP-qPCR analyses.

DNA-fluorescence *in situ* hybridization (FISH) and Imaging

DNA-FISH analysis was performed as previously described (Kondo et al., 2014; Yakushiji-Kaminatsui et al., 2016). Confocal images were captured with 65 nm pixels in *xy* and 300 nm steps in the *z*-plane by microscopy (Olympus UPlanSApo 1003 NA 1.40 and PlanApo N 603 NA1.42). We deconvoluted the images and measured the distances of foci using the Volocity application (Improvision). *P*-values were determined by χ^2 test.

Chromatin immunoprecipitation (ChIP), ChIP-qPCR and ChIP-seq

Micro-dissected proximal and distal forelimb buds at E10.5 from wild-type (BDF2) embryos treated with vehicle or ATRA (+RA), *Cyp26b1*$^{+/+}$ (wild type) and *Cyp26b1*$^{-/-}$ and distal forelimb buds at E10.5 from *Pcgf3*$^{fl/fl}$;*Pcgf5*$^{fl/fl}$ (control) or *ERT2-Cre; Pcgf3*$^{fl/fl}$;*Pcgf5*$^{fl/fl}$ embryos were used for ChIP-qPCR. The most proximal (*Meis2*-expressing domain) and distal tips of forelimb buds at E11.5 from wild-type (CD1) embryos were used for ChIP-seq. ChIP was performed as described previously (Yakushiji-Kaminatsui et al., 2016). For each immunoprecipitation, anti-RING1B (Atsuta et al., 2001), anti-H3K27me3 (07-449, Millipore), anti-H3K4me3 (07-473, Millipore), anti-H3K27ac (ab4729, Abcam) and anti-RAR (sc-773X, Santa Cruz) were used. ChIP-qPCR was performed on an Mx3005P system using the Brilliant SYBR Green QPCR Master Mix (Agilent Technologies). ChIP-qPCR analysis using RING1B/H3K27me3 and H3K4me3/H3K27ac (except for *Pcgf3/5* mutant embryos) was carried out with three or two biological replicates, respectively. ChIP-qPCR analysis using *Pcgf3/5* mutant was performed with six biological replicates. Primer sequences are listed in Table S1. For ChIP-Seq, at least 5 ng of purified DNA was used to make libraries and the material was sequenced with 100-bp single-end reads on an Illumina Hiseq2500 according to the manufacturer's protocol (Illumina).

ChIP-seq data analysis

Demultiplexed ChIP-seq reads were mapped onto the mm10 or hg19 using Bowtie (Version 0.12.7) (Langmead et al., 2009), with parameters '-m1 –strata –best' according to conditions described previously (Riising et al., 2014), and PCR duplicates were removed from mapped reads using SAMtools (Version 0.1.18) (Li et al., 2009). All ChIP-seq data shown in this research were normalized to get a 1× depth of coverage by using bamCoverage (Version 2.5.0), and the difference (subtraction of vehicle from treated samples of the normalized number of reads in Fig. S1A) was analyzed using bamCompare (Version 2.5.0) (Ramírez et al., 2014, 2016). All analysis was performed with the Denis Duboule lab Galaxy server (the Bioteam Appliance Galaxy Edition, bioteam.net, bioteam.net/products/galaxy-appliance) (Afgan et al., 2016). For Fig. S1, H3K27ac and RAR ChIP-seq data before and after tamibarotene treatment of human AML cells were obtained from the NCBI SRA database (SRP103029, see also Table S2). For Fig. S1B, short reads were aligned on the human genome (NCBI version 38) using bowtie2 (version 2.3.4) with default options and significantly enriched regions were detected using MACS2 (version 2.1.0) with an option to process broad peaks. Overlaps between RAR and H3K27ac were evaluated using inclusion of RAR and/or H3K27ac peaks in merged broad peaks that had significantly enriched and at least more than twice the number of reads than whole cell extract. RPKM values in all merged regions were calculated for all experiments and changes after tamibarotene treatment were evaluated.

Mathematical modeling and simulation

We tested the network model (shown in Fig. 2D) to see if it could account for the expression patterns of *Meis1/2*, *Fgf8* and *Hoxa13* in ATRA-treated wild-type (+RA), *Ring1A/B*-dKO or *Ring1A/B;Meis2*-tKO forelimb buds at E10.5. We did not consider the impact of tissue growth, as the time scale of tissue growth is considerably slower than chemical reactions or diffusions. We sought to recapitulate the gene expression pattern at E10.5 (see Probst et al., 2011) by focusing on the RA-FGF gradient in the forelimb bud. We assumed that enzymatic reactions, such as association/dissociation between RA and its receptors and between transcription factors and their binding regions, are at equilibrium as time scales of these reactions are much quicker than those of gene expression.

Our mathematical model is based on a set of reaction-diffusion type partial differential equations for RA (R), *Meis1/2* (M), FGF8 (F), CYP26B1 (C) and *Hoxa13* (H) (see Fig. 2D for the network model):

$$\frac{\partial R}{\partial t} = D_R \Delta R - (\gamma_R + \gamma_{RC} C) R, \tag{1}$$

$$\frac{\partial F}{\partial t} = D_F \Delta F - \gamma_F F,\ F_0 \propto \frac{K_{FM}^h}{M^h + K_{FM}^h}, \tag{2}$$

$$\frac{\partial C}{\partial t} = \alpha_C \frac{F^h}{F^h + K_{CF}^h} \frac{K_{CM}^h}{M^h + K_{CM}^h} - \gamma_C C, \tag{3}$$

$$\frac{\partial M}{\partial t} = \alpha_M \frac{R^h}{R^h + K_{MR}(P)^h} - \gamma_M M, \tag{4}$$

$$\frac{\partial H}{\partial t} = \alpha_H \frac{K_{HM}^h}{M^h + K_{HM}^h} - \gamma_H H \tag{5}$$

The expression of *Ring1A* or *Ring1B* did not change between proximal and distal regions of the forelimb bud (Yakushiji-Kaminatsui et al., 2016). Thus, in our model the expression level of PcG proteins was constant (P). RING1A/B regulated proximal gene expression by competing with RA signaling. RA is inactivated by CYP26B1 and all variables decay linearly at rate γ_*. The expression of proximal genes, CYP26B1, and distal genes were modeled by a Hill-type function with maximum production rates α_*. Expression of the proximal genes (here, we considered both *Meis2* and *Meis1* as proximal genes because of their potential redundancy) is competitively regulated by RA and PcG proteins. RA and FGF8 are produced in the flank and in the AER, respectively, and both diffuse into the forelimb bud mesenchyme with a diffusion constant D_*. In this simulation, we used a fixed value of RA (R_0) at the flank. We assumed FGF8 influx from the AER was negatively regulated by Meis1/2 based on our previous results. The *Fgf8* expression at the AER was downregulated in the *Ring1A/B*-dKO but was considerably restored in the *Ring1A/B;Meis2*-tKO mutants (Yakushiji-Kaminatsui et al., 2016). Zero-flux conditions were applied to other boundaries. We also assumed that Meis1/2 suppresses *Hoxa13*. *Meis2* and *Hoxa13* show complementary expression patterns in different conditions [e.g. in wild type or control (*Ring1A*-KO), ATRA-treated wild

type (+RA) and *Ring1* mutants] and downregulation of *Hoxa13* in the *Ring1A/B*-dKO was considerably restored in the *Ring1A/B;Meis2*-tKO mutants (Yakushiji-Kaminatsui et al., 2016). This is further supported by our unpublished observations showing Meis2 binding to the *Hoxa13* or *Cyp26b1* promoters (T.K. and H.K., unpublished observations) and another study showing a PcG-mediated interaction of the *Meis2* gene locus with the *HoxA* cluster in mouse embryonic stem cells (Schoenfelder et al., 2015).

Computer simulations were performed by applying the following relative values to respective components of equations. For RA and FGF8, normalized concentrations relative to their source levels were used (for FGF8, normalization by the source value was carried out for M=0). The values of K_* in Hill functions were chosen so that the expression patterns of CYP26B1, proximal and distal genes at the equilibrium, were similar to those observed in the wild type. Hill coefficients (h) were set to 2, and simulation results remained mostly unchanged for values other than 2. For *Ring1A/B*-dKO and *Ring1A/B;Meis2*-tKO, a smaller value for $K_{MR}(P)$ compared with the wild type was adopted (see Table 1 for parameters). For *Ring1A/B;Meis2*-tKO, the value of α_M was also set to be smaller than the wild type, but was not zero as *Meis1* is still expressed. For ATRA treatment, a larger value for the source level of RA was used.

Acknowledgements
We thank Dr Janet Rossant (The Hospital for Sick Children, Canada) and Dr Hiroshi Hamada (RIKEN, Japan) for providing *RARE-lacZ* and *Cyp26b1*$^{+/-}$ mice, respectively, and our animal facility group staffs for animal care and two-cell transplantations to foster mothers. We deeply appreciate Dr Denis Duboule for his generous support.

Competing interests
The authors declare no competing or financial interests.

Author contributions
Conceptualization: N.Y.-K., Y.M., H.K.; Methodology: N.Y.-K., T.K., K.H., Y.M., H.K.; Formal analysis: N.Y.-K., K.H., T.A.E., O.O., Y.M.; Investigation: N.Y.-K., T.K., J.S., O.M., H.K.; Resources: M.N., Y.K., K.K., M.V.; Writing - original draft: N.Y.-K., Y.M., H.K.; Writing - review & editing: J.S.; Supervision: H.K.; Funding acquisition: N.Y.-K., T.K., H.K.

Funding
This work was supported by Grants-in-Aid for Scientific Research from the Ministry of Education, Culture, Sports, Science and Technology of Japan (MEXT) (23249015 to H.K.), the Japan Agency for Medical Research and Development (AMED) (JP18gm0510016 to H.K. and T.K.), the Special Postdoctoral Researcher Program of RIKEN (to N.Y.-K.), the Regional Innovation Program from MEXT (to T.K.) and the Cross-ministerial Strategic Innovation Promotion Program (SIP) from Cabinet Office, Government of Japan (to T.K. and H.K.).

Data availability
Our ChIP-seq data set is available from the NCBI Gene Expression Omnibus repository under accession number GSE105206. The public ChIP-seq datasets used in this study are listed in Table S2.

Supplementary information
Supplementary information available online at
http://dev.biologists.org/lookup/doi/10.1242/dev.166348.supplemental

References
Afgan, E., Baker, D., van den Beek, M., Blankenberg, D., Bouvier, D., Čech, M., Chilton, J., Clements, D., Coraor, N., Eberhard, C. et al. (2016). The Galaxy platform for accessible, reproducible and collaborative biomedical analyses: 2016 update. *Nucleic Acids Res.* **44**, W3-W10.

Akasaka, T., van Lohuizen, M., van der Lugt, N., Mizutani-Koseki, Y., Kanno, M., Taniguchi, M., Vidal, M., Alkema, M., Berns, A. and Koseki, H. (2001). Mice doubly deficient for the Polycomb group genes Mel18 and Bmi1 reveal synergy and requirement for maintenance but not initiation of Hox gene expression. *Development* **128**, 1587-1597.

Akimaru, H., Chen, Y., Dai, P., Hou, D.-X., Nonaka, M., Smolik, S. M., Armstrong, S., Goodman, R. H. and Ishii, S. (1997). Drosophila CBP is a co-activator of cubitus interruptus in hedgehog signalling. *Nature* **386**, 735-738.

Almeida, M., Pintacuda, G., Masui, O., Koseki, Y., Gdula, M., Cerase, A., Brown, D., Mould, A., Innocent, C., Nakayama, M. et al. (2017). PCGF3/5-PRC1 initiates Polycomb recruitment in X chromosome inactivation. *Science* **356**, 1081-1084.

Aranda, S., Mas, G. and Di Croce, L. (2015). Regulation of gene transcription by Polycomb proteins. *Sci. Adv.* **1**, e1500737.

Atsuta, T., Fujimura, S., Moriya, H., Vidal, M., Akasaka, T. and Koseki, H. (2001). Production of monoclonal antibodies against mammalian Ring1B proteins. *Hybridoma* **20**, 43-46.

Bajpe, P. K., Heynen, G. J. J. E., Mittempergher, L., Grernrum, W., de Rink, I. A., Nijkamp, W., Beijersbergen, R. L., Bernards, R. and Huang, S. (2013). The corepressor CTBP2 is a coactivator of retinoic acid receptor/retinoid X receptor in retinoic acid signaling. *Mol. Cell. Biol.* **33**, 3343-3353.

Bel-Vialar, S., Coré, N., Terranova, R., Goudot, V., Boned, A. and Djabali, M. (2000). Altered retinoic acid sensitivity and temporal expression of Hox genes in polycomb-M33-deficient mice. *Dev. Biol.* **224**, 238-249.

Blackledge, N. P., Farcas, A. M., Kondo, T., King, H. W., McGouran, J. F., Hanssen, L. L. P., Ito, S., Cooper, S., Kondo, K., Koseki, Y. et al. (2014). Variant PRC1 complex-dependent H2A ubiquitylation drives PRC2 recruitment and polycomb domain formation. *Cell* **157**, 1445-1459.

Blackledge, N. P., Rose, N. R. and Klose, R. J. (2015). Targeting Polycomb systems to regulate gene expression: modifications to a complex story. *Nat. Rev. Mol. Cell Biol.* **16**, 643-649.

Boukarabila, H., Saurin, A. J., Batsché, E., Mossadegh, N., van Lohuizen, M., Otte, A. P., Pradel, J., Muchardt, C., Sieweke, M. et al. (2009). The PRC1 Polycomb group complex interacts with PLZF/RARA to mediate leukemic transformation. *Genes Dev.* **23**, 1195-1206.

Capdevila, J., Tsukui, T., Esteban, C. R., Zappavigna, V. and Belmonte, J. C. I. (1999). Control of vertebrate limb outgrowth by the proximal factor Meis2 and distal antagonism of BMPs by Gremlin. *Mol. Cell* **4**, 839-849.

Chatagnon, A., Veber, P., Morin, V., Bedo, J., Triqueneaux, G., Sémon, M., Laudet, V., d'Alché-Buc, F. and Benoit, G. (2015). RAR/RXR binding dynamics distinguish pluripotency from differentiation associated cis-regulatory elements. *Nucleic Acids Res.* **43**, 4833-4854.

Chen, H., Lin, R. J., Schiltz, R. L., Chakravarti, D., Nash, A., Nagy, L., Privalsky, M. L., Nakatani, Y. and Evans, R. M. (1997). Nuclear receptor coactivator ACTR is a novel histone acetyltransferase and forms a multimeric activation complex with P/CAF and CBP/p300. *Cell* **90**, 569-580.

Chen, W., Jia, W., Wang, K., Si, X., Zhu, S., Duan, T. and Kang, J. (2013). Distinct roles for CBP and p300 on the RA-mediated expression of the meiosis commitment gene Stra8 in mouse embryonic stem cells. *PLoS ONE* **8**, e66076.

Cunningham, T. J. and Duester, G. (2015). Mechanisms of retinoic acid signalling and its roles in organ and limb development. *Nat. Rev. Mol. Cell Biol.* **16**, 110-123.

Cunningham, T. J., Zhao, X., Sandell, L. L., Evans, S. M., Trainor, P. A. and Duester, G. (2013). Antagonism between retinoic acid and fibroblast growth factor signaling during limb development. *Cell Rep* **3**, 1503-1511.

Endoh, M., Endo, T. A., Shinga, J., Hayashi, K., Farcas, A., Ma, K. W., Ito, S., Sharif, J., Endoh, T., Onaga, N. et al. (2017). PCGF6-PRC1 suppresses premature differentiation of mouse embryonic stem cells by regulating germ cell-related genes. *Elife* **6**, e21064.

Farcas, A. M., Blackledge, N. P., Sudbery, I., Long, H. K., McGouran, J. F., Rose, N. R., Lee, S., Sims, D., Cerase, A., Sheahan, T. W. et al. (2012). KDM2B links the polycomb repressive complex 1 (PRC1) to recognition of CpG islands. *Elife* **1**, e00205.

Gaarenstroom, T. and Hill, C. S. (2014). TGF-β signaling to chromatin: How Smads regulate transcription during self-renewal and differentiation. *Semin. Cell Dev. Biol.* **32**, 107-118.

Gao, Z., Zhang, J., Bonasio, R., Strino, F., Sawai, A., Parisi, F., Kluger, Y. and Reinberg, D. (2012). PCGF homologs, CBX proteins, and RYBP define functionally distinct PRC1 family complexes. *Mol. Cell* **45**, 344-356.

He, J., Shen, L., Wan, M., Taranova, O., Wu, H. and Zhang, Y. (2013). Kdm2b maintains murine embryonic stem cell status by recruiting PRC1 complex to CpG islands of developmental genes. *Nat. Cell Biol.* **15**, 373-384.

Isono, K., Fujimura, Y., Shinga, J., Yamaki, M., O-Wang, J., Takihara, Y., Murahashi, Y., Takada, Y., Mizutani-Koseki, Y. and Koseki, H. (2005). Mammalian polyhomeotic homologues Phc2 and Phc1 act in synergy to mediate polycomb repression of Hox genes. *Mol. Cell. Biol.* **25**, 6694-6706.

Isono, K., Endo, T. A., Ku, M., Yamada, D., Suzuki, R., Sharif, J., Ishikura, T., Toyoda, T., Bernstein, B. E. and Koseki, H. (2013). SAM domain polymerization links subnuclear clustering of PRC1 to gene silencing. *Dev. Cell* **26**, 565-577.

Itoh, S., Ericsson, J., Nishikawa, J., Heldin, C.-H. and ten Dijke, P. (2000). The transcriptional co-activator P/CAF potentiates TGF-β/Smad signaling. *Nucleic Acids Res.* **28**, 4291-4298.

Jin, Q., Yu, L.-R., Wang, L., Zhang, Z., Kasper, L. H., Lee, J.-E., Wang, C., Brindle, P. K., Dent, S. Y. R. and Ge, K. (2011). Distinct roles of GCN5/PCAF-mediated H3K9ac and CBP/p300-mediated H3K18/27ac in nuclear receptor transactivation. *EMBO J.* **30**, 249-262.

Kondo, T., Isono, K., Kondo, K., Endo, T. A., Itohara, S., Vidal, M. and Koseki, H. (2014). Polycomb potentiates meis2 activation in midbrain by mediating interaction of the promoter with a tissue-specific enhancer. *Dev. Cell* **28**, 94-101.

Kondo, T., Ito, S. and Koseki, H. (2016). Polycomb in transcriptional phase transition of developmental genes. *Trends Biochem. Sci.* **41**, 9-19.

Langmead, B., Trapnell, C., Pop, M. and Salzberg, S. L. (2009). Ultrafast and memory-efficient alignment of short DNA sequences to the human genome. *Genome Biol.* **10**, R25.
Lehninger, A. L. (1970). *Biochemistry: the molecular basis of cell structure and function*. New York: Worth Publishers.
Leid, M., Kastner, P. and Chambon, P. (1992). Multiplicity generates diversity in the retinoic acid signalling pathways. *Trends Biochem. Sci.* **17**, 427-433.
Li, H., Handsaker, B., Wysoker, A., Fennell, T., Ruan, J., Homer, N., Marth, G., Abecasis, G. and Durbin, R. (2009). The sequence alignment/map format and SAMtools. *Bioinformatics* **25**, 2078-2079.
Loughna, S. and Henderson, D. (2007). Methodologies for staining and visualisation of beta-galactosidase in mouse embryos and tissues. *Methods Mol. Biol.* **411**, 1-11.
Mangelsdorf, D. J. and Evans, R. M. (1995). The RXR heterodimers and orphan receptors. *Cell* **83**, 841-850.
Marino, S. (2005). Medulloblastoma: developmental mechanisms out of control. *Trends Mol. Med.* **11**, 17-22.
McKeown, M. R., Corces, M. R., Eaton, M. L., Fiore, C., Lee, E., Lopez, J. T., Chen, M. W., Smith, D., Chan, S. M., Koenig, J. L. et al. (2017). Superenhancer analysis defines novel epigenomic subtypes of non-APL AML, including an RARα dependency targetable by SY-1425, a potent and selective RARα agonist. *Cancer Discov.* **7**, 1136-1153.
Mercader, N., Leonardo, E., Piedra, M. E., Martinez, A. C., Ros, M. A. and Torres, M. (2000). Opposing RA and FGF signals control proximodistal vertebrate limb development through regulation of Meis genes. *Development* **127**, 3961-3970.
Mercader, N., Selleri, L., Criado, L. M., Pallares, P., Parras, C., Cleary, M. L. and Torres, M. (2009). Ectopic Meis1 expression in the mouse limb bud alters P-D patterning in a Pbx1-independent manner. *Int. J. Dev. Biol.* **53**, 1483-1494.
Nagy, L., Kao, H.-Y., Chakravarti, D., Lin, R. J., Hassig, C. A., Ayer, D. E., Schreiber, S. L. and Evans, R. M. (1997). Nuclear receptor repression mediated by a complex containing SMRT, mSin3A, and histone deacetylase. *Cell* **89**, 373-380.
Parr, B. A. and McMahon, A. P. (1995). Dorsalizing signal Wnt-7a required for normal polarity of D-V and A-P axes of mouse limb. *Nature* **374**, 350-353.
Pintacuda, G., Wei, G., Roustan, C., Kirmizitas, B. A., Solcan, N., Cerase, A., Castello, A., Mohammed, S., Moindrot, B., Nesterova, T. B. et al. (2017). hnRNPK recruits PCGF3/5-PRC1 to the Xist RNA B-repeat to establish polycomb-mediated chromosomal silencing. *Mol. Cell* **68**, 955-969 e10.
Probst, S., Kraemer, C., Demougin, P., Sheth, R., Martin, G. R., Shiratori, H., Hamada, H., Iber, D., Zeller, R. and Zuniga, A. (2011). SHH propagates distal limb bud development by enhancing CYP26B1-mediated retinoic acid clearance via AER-FGF signalling. *Development* **138**, 1913-1923.
Ramírez, F., Dündar, F., Diehl, S., Grüning, B. A. and Manke, T. (2014). deepTools: a flexible platform for exploring deep-sequencing data. *Nucleic Acids Res.* **42**, W187-W191.
Ramírez, F., Ryan, D. P., Grüning, B., Bhardwaj, V., Kilpert, F., Richter, A. S., Heyne, S., Dündar, F. and Manke, T. (2016). deepTools2: a next generation web server for deep-sequencing data analysis. *Nucleic Acids Res.* **44**, W160-W165.
Riising, E. M., Comet, I., Leblanc, B., Wu, X., Johansen, J. V. and Helin, K. (2014). Gene silencing triggers polycomb repressive complex 2 recruitment to CpG islands genome wide. *Mol. Cell* **55**, 347-360.
Roose, J., Molenaar, M., Peterson, J., Hurenkamp, J., Brantjes, H., Moerer, P., van de Wetering, M., Destrée, O. and Clevers, H. (1998). The *Xenopus* Wnt effector XTcf-3 interacts with Groucho-related transcriptional repressors. *Nature* **395**, 608-612.
Rosello-Diez, A., Arques, C. G., Delgado, I., Giovinazzo, G. and Torres, M. (2014). Diffusible signals and epigenetic timing cooperate in late proximo-distal limb patterning. *Development* **141**, 1534-1543.
Rossant, J., Zirngibl, R., Cado, D., Shago, M. and Giguere, V. (1991). Expression of a retinoic acid response element-hsplacZ transgene defines specific domains of transcriptional activity during mouse embryogenesis. *Genes Dev.* **5**, 1333-1344.
Sánchez, C., Sánchez, I., Demmers, J. A. A., Rodriguez, P., Strouboulis, J. and Vidal, M. (2007). Proteomics analysis of Ring1B/Rnf2 interactors identifies a novel complex with the Fbxl10/Jhdm1B histone demethylase and the Bcl6 interacting corepressor. *Mol. Cell. Proteomics* **6**, 820-834.
Schoenfelder, S., Sugar, R., Dimond, A., Javierre, B.-M., Armstrong, H., Mifsud, B., Dimitrova, E., Matheson, L., Tavares-Cadete, F., Furlan-Magaril, M. et al. (2015). Polycomb repressive complex PRC1 spatially constrains the mouse embryonic stem cell genome. *Nat. Genet.* **47**, 1179-1186.
Sewalt, R. G. A. B., Gunster, M. J., van der Vlag, J., Satijn, D. P. E. and Otte, A. P. (1999). C-Terminal binding protein is a transcriptional repressor that interacts with a specific class of vertebrate Polycomb proteins. *Mol. Cell. Biol.* **19**, 777-787.
Simon, J. A. and Kingston, R. E. (2009). Mechanisms of polycomb gene silencing: knowns and unknowns. *Nat. Rev. Mol. Cell Biol.* **10**, 697-708.
Tie, F., Banerjee, R., Stratton, C. A., Prasad-Sinha, J., Stepanik, V., Zlobin, A., Diaz, M. O., Scacheri, P. C. and Harte, P. J. (2009). CBP-mediated acetylation of histone H3 lysine 27 antagonizes Drosophila Polycomb silencing. *Development* **136**, 3131-3141.
Uzkudun, M., Marcon, L. and Sharpe, J. (2015). Data-driven modelling of a gene regulatory network for cell fate decisions in the growing limb bud. *Mol. Syst. Biol.* **11**, 815.
van der Vlag, J. and Otte, A. P. (1999). Transcriptional repression mediated by the human polycomb-group protein EED involves histone deacetylation. *Nat. Genet.* **23**, 474-478.
Vargesson, N., Kostakopoulou, K., Drossopoulou, G., Papageorgiou, S. and Tickle, C. (2001). Characterisation of hoxa gene expression in the chick limb bud in response to FGF. *Dev. Dyn. Off. Publ. Am. Assoc. Anat.* **220**, 87-90.
Wilkinson, D. G. and Nieto, M. A. (1993). Detection of messenger RNA by in situ hybridization to tissue sections and whole mounts. *Methods Enzymol.* **225**, 361-373.
Wu, X., Johansen, J. V. and Helin, K. (2013). Fbxl10/Kdm2b recruits polycomb repressive complex 1 to CpG islands and regulates H2A ubiquitylation. *Mol. Cell* **49**, 1134-1146.
Yakushiji-Kaminatsui, N., Kondo, T., Endo, T. A., Koseki, Y., Kondo, K., Ohara, O., Vidal, M. and Koseki, H. (2016). RING1 proteins contribute to early proximal-distal specification of the forelimb bud by restricting Meis2 expression. *Development* **143**, 276-285.
Yashiro, K., Zhao, X., Uehara, M., Yamashita, K., Nishijima, M., Nishino, J., Saijoh, Y., Sakai, Y. and Hamada, H. (2004). Regulation of retinoic acid distribution is required for proximodistal patterning and outgrowth of the developing mouse limb. *Dev. Cell* **6**, 411-422.
Yokobayashi, S., Liang, C.-Y., Kohler, H., Nestorov, P., Liu, Z., Vidal, M., van Lohuizen, M., Roloff, T. C. and Peters, A. H. (2013). PRC1 coordinates timing of sexual differentiation of female primordial germ cells. *Nature* **495**, 236-240.
Zhao, W., Huang, Y., Zhang, J., Liu, M., Ji, H., Wang, C., Cao, N., Li, C., Xia, Y., Jiang, Q. et al. (2017). Polycomb group RING finger proteins 3/5 activate transcription via an interaction with the pluripotency factor Tex10 in embryonic stem cells. *J. Biol. Chem.* **292**, 21527-21537.

Supplemental Table S1

Table S1. Primer information

For genotyping		5' ->3'
Pcgf3	P1	ATAAGATGAGATGGGATGGGC
	P2	ACGCCTCCAGGTGATCCATAC
Pcgf5	P1	TGTTTACAGAGAGGAAGCGCC
	P2	TGGCCTTGGTACACATATAGC

For ChIP-qPCR		5' ->3'
Meis1	Previously described in Yakushiji-Kaminatsui et al., 2016	
Meis2		
Hoxa11 promoter	Forward	CTCGCACCTTGTACCCTGAT
	Reverse	GATGCCGATTGCGTTTAGTT
Hoxa13 promoter	Forward	TCCTGGAACCAACAGGAAAC
	Reverse	TGGCATGTTTTAGGGACCTC
Pitx2 promoter	Forward	ATTTCTCCAGGAGCCATTTG
	Reverse	ACTCTCTGTCGTCGGGAGTC

Supplemental Table S2

Table S2. Public ChIP-seq datasets used in this research

Dataset	Accession number	Reference
E11.5, forelimb proximal, RING1B	GSM1716759	Yakushiji-Kaminatsui et al., RING1 proteins contribute to early proximal-distal specification of the forelimb bud by restricting Meis2 expression, **2016** Development 143, 276-285.
E11.5, forelimb distal, RING1B	GSM1716760	
MV-4-11, Vehicle 1, RARA WCE	SRX2705416	McKeown et al., Superenhancer Analysis Defines Novel Epigenomic Subtypes of Non-APL AML, Including an RARα Dependency Targetable by SY-1425, a Potent and Selective RARα Agonist, **2017** Cancer Discov. 10, 1136-1153.
MV-4-11, Vehicle 2, RARA WCE	SRX2705415	
MV-4-11, Vehicle 1, RARA IP	SRX2705441	
MV-4-11, Vehicle 2, RARA IP	SRX2705440	
MV-4-11, Treated 1, RARA WCE	SRX2705418	
MV-4-11, Treated 2, RARA WCE	SRX2705417	
MV-4-11, Treated 1, RARA IP	SRX2705443	
MV-4-11, Treated 2, RARA IP	SRX2705442	
MV-4-11, Vehicle 1, H3K27ac WCE	SRX2705477	
MV-4-11, Vehicle 2, H3K27ac WCE	SRX2705476	
MV-4-11, Vehicle 3, H3K27ac WCE	SRX2705474	
MV-4-11, Vehicle 1, H3K27ac IP	SRX2705454	
MV-4-11, Vehicle 2, H3K27ac IP	SRX2705453	
MV-4-11, Vehicle 3, H3K27ac IP	SRX2705450	
MV-4-11, Treated 2, H3K27ac WCE	SRX2705478	
MV-4-11, Treated 3, H3K27ac WCE	SRX2705475	
MV-4-11, Treated 2, H3K27ac IP	SRX2705455	
MV-4-11, Treated 3, H3K27ac IP	SRX2705452	
MV-4-11, Treated 4, H3K27ac IP	SRX2705451	

Supplemental Figures

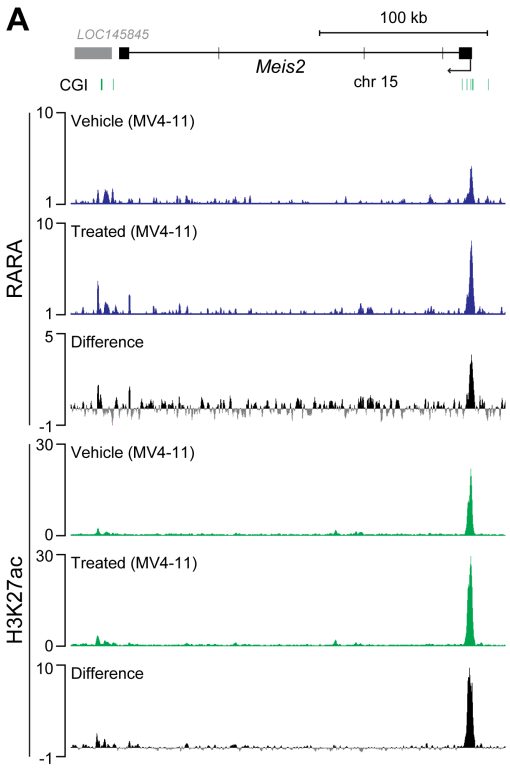

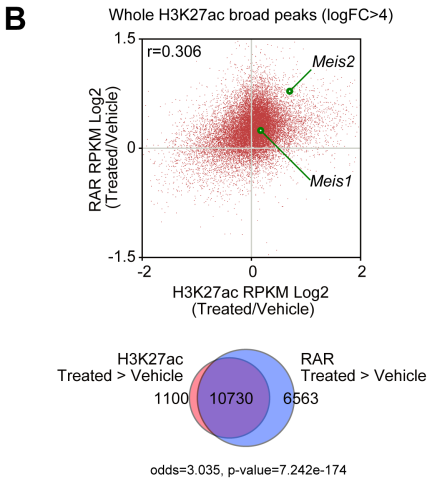

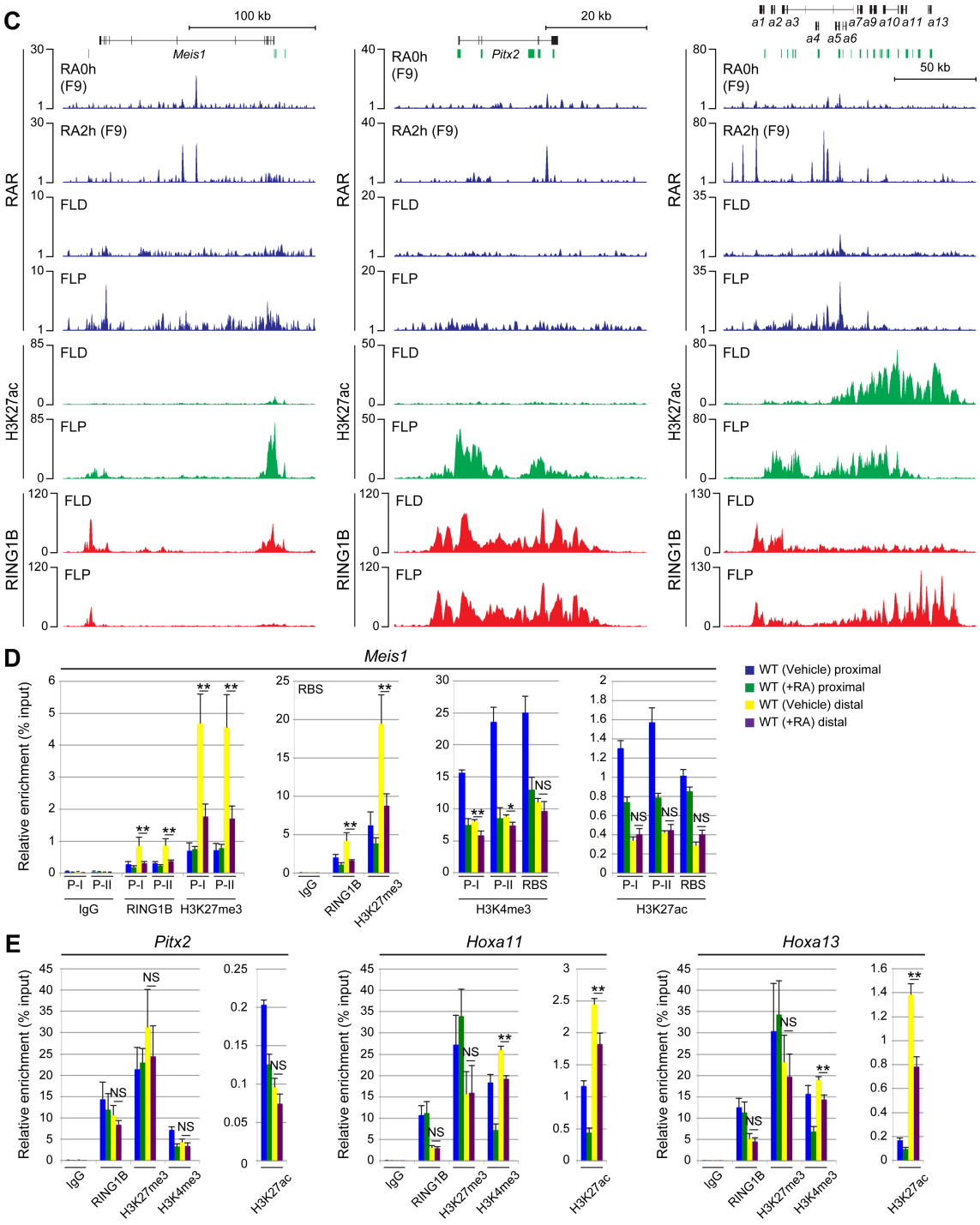

Fig. S1 (related to Fig. 1). Effects of either SY-1425 (tamibarotene) or ATRA on RARα, histone modification and RING1B activities in human MV4-11 cells or mouse forelimb buds at E10.5.

(A) ChIP-seq showing the level of RARA and H3K27ac at *Meis2* locus in MV4-11 cells treated with vehicle or SY-1425, a selective RARα agonist (treated). The difference in the normalized number of reads between the vehicle- and SY1425-treated is shown by negative (gray) and positive (black), respectively (tracks 3 and 6). (B) Scatter plots representing the logarithmic ratio of normalized read counts between SY-1524 stimulated and vehicle-treated MV4-11 cells (top). The alterations in enrichments of H3K27ac and RAR by SY-1425 treatment showed a positive correlation. Overlaps between peaks of RAR and H3K27ac that had significantly enriched and at least more than 2 times reads as compared with whole cell extract (bottom). (C) Distribution of RAR, H3K27ac and RING1B at the *Meis1* (left), *Pitx2* (middle) and *HoxA* (right) locus in F9 cells (0 hour with only vehicle (RA0h)) and 2 hours after RA stimulation (RA2h), E11.5 proximal (FLP) and distal (FLD) forelimb buds revealed by ChIP-seq analysis. (D, E) ChIP-qPCR analysis showing the levels of RING1B, H3K27me3, H3K4me3 and H3K27ac at the TSS and RBS of the *Meis1* (D) and the promoters of *Hoxa11*, *Hoxa13* and *Pitx2* (E) in the proximal and distal regions of E10.5 forelimb buds from wild type (vehicle) and ATRA-treated wild type (+RA) embryos. Error bars indicate s.e.m. of two or three biological replicates. **P<0.01, *P<0.05, NS>0.05, Student's *t*-test. Enrichment of ChIP-seq (*Y*-axis) in (A) and (C) is shown as the normalized depth of coverage.

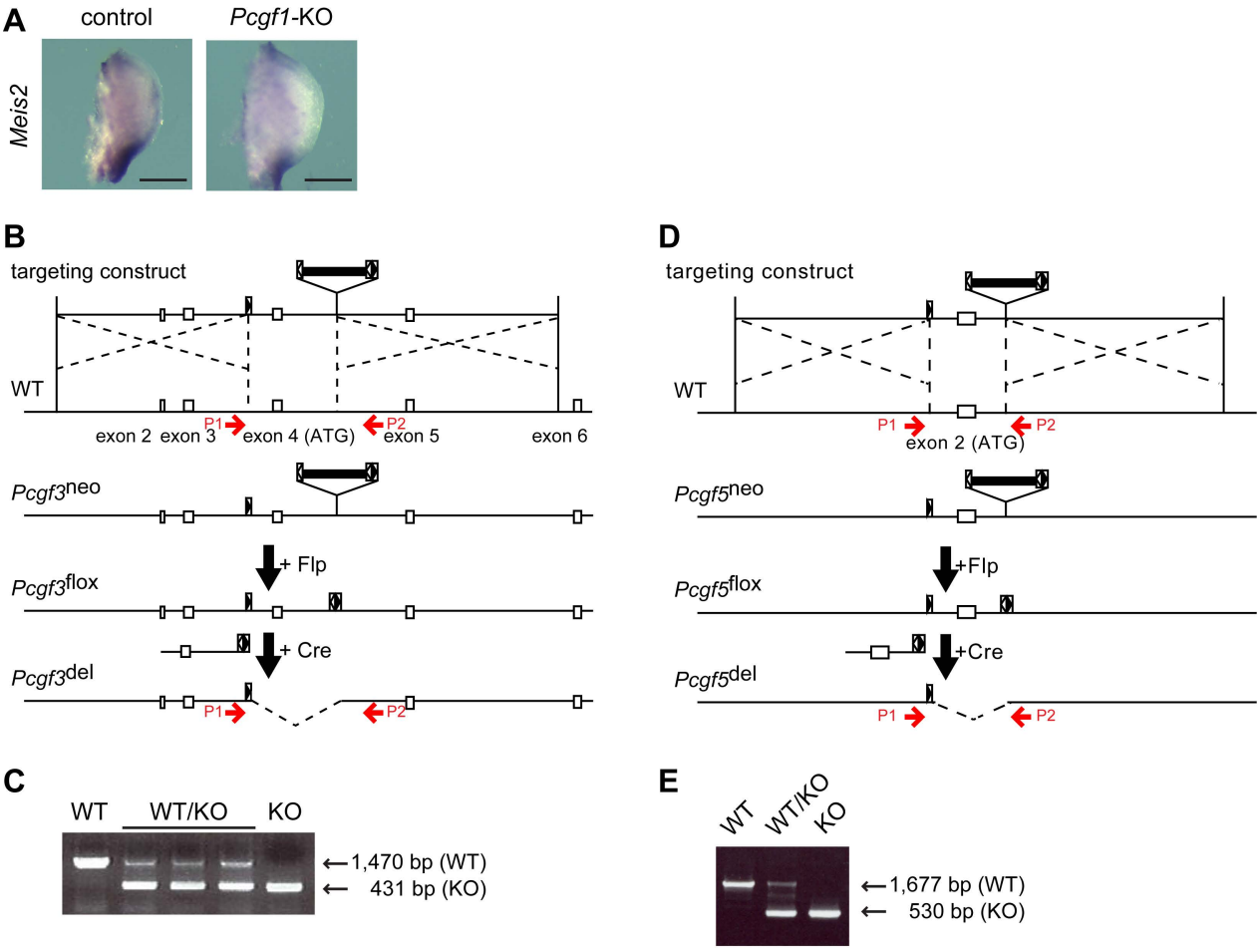

Fig. S2 (related to Fig. 3). *Meis2* expression in *Pcgf1*-KO forelimb buds and Generation of *Pcgf3/5* mutants. (A) *Meis2* expression in control (*Pcgf1*$^{fl/fl}$) and *Pcgf1*-KO forelimb buds at E10.5. Scale bar, 250 µm. (B) Schematic representation of gene targeting strategy to delete *Pcgf3*. Targeting construct to generate the *Pcgf3*^{neo} allele harbors a Neomycin resistant gene cassette (indicated by bold bars), two loxP sites (indicated by closed triangles) and two FRT (open triangles) sites. The Neomycin resistant gene cassette was removed by mating *Pcgf3*$^{neo/+}$ with FLP deleter line (CAG-FLP) to generate the *Pcgf3*^{flox} allele. The *Pcgf3*-KO allele was generated by deleting the 4th exon of *Pcgf3* by crossing mice carrying *Pcgf3*^{flox} with CAG-Cre mouse strain. The *Pcgf3* mutant line was maintained as heterozygotes and KO mice were obtained by mating *Pcgf3*$^{+/-}$ female with *Pcgf3*$^{+/-}$ male. Genomic positions of PCR primers (P1 and

P2) used for genotyping are indicated by red arrows. (C) PCR analysis to distinguish the wild type (WT), *Pcgf3*$^{+/-}$ (WT/KO) and *Pcgf3*$^{-/-}$ (KO). (D) Schematic representation of gene targeting strategy to delete *Pcgf5*. Targeting construct to generate the *Pcgf5*^{neo} allele harbors a Neomycin resistant gene cassette (indicated by bold bars), two loxP sites (indicated by closed triangles) and two FRT (open triangles) sites. The Neomycin resistant gene cassette was removed by mating *Pcgf5*$^{neo/+}$ with FLP deleter line (CAG-FLP) to generate the *Pcgf5*^{flox} allele. The *Pcgf5*-KO allele was generated by deleting the 2nd exon of *Pcgf5* by crossing mice carrying *Pcgf5*^{flox} with CAG-Cre mouse strain. The *Pcgf5* mutant line was maintained as heterozygotes and KO mice were obtained by mating *Pcgf5*$^{+/-}$ female with *Pcgf5*$^{+/-}$ male. Genomic positions of PCR primers (P1 and P2) used for genotyping are indicated by red arrows. (E) PCR analysis to distinguish the wild type (WT), *Pcgf5*$^{+/-}$ (WT/KO) and *Pcgf5*$^{-/-}$ (KO).